

J507 堆焊层超声冲击表面纳米化

李 东, 樊 钊, 廖礼宝, 张 莉*

(华东理工大学 化学工程联合国家重点实验室, 上海 200237)

摘 要: 采用在工程上获得广泛应用的超声冲击技术在 J507 堆焊层上制备纳米结构表层, 利用金相显微镜、X 射线衍射和透射电子显微镜表征了表面纳米晶层的结构, 并对超声冲击表面纳米化处理前后表面层显微硬度的变化进行了分析。结果表明, 经过超声冲击处理后, 试样表层的晶粒可细化至 21.25 nm。在超声冲击载荷作用下, 粗晶粒内部形成高密度的位错墙和位错缠结, 位错墙和位错缠结逐渐演变成小角度亚晶界, 小角度亚晶界继续吸收位错而转变成大角度晶界, 亚晶内部不断重复上述过程, 使晶粒尺寸不断减小, 最终形成纳米晶。表面强化层的厚度为 100 μm 。与样品的心部相比, 表面纳米晶层的显微硬度提高 1.4 倍。

关键词: 堆焊层; 超声冲击; 表面纳米化; 显微硬度

中图分类号: TG441.8 **文献标识码:** A **文章编号:** 0253-360X(2009)01-0101-04



李 东

0 序 言

焊接熔池凝固过程中, 发生交互结晶形成晶粒粗大的非平衡铸态树枝晶。这种粗大显微组织是造成焊接接头性能恶化的主要原因之一。因此, 如何通过细化晶粒提高焊缝组织性能一直是焊接工作者关注的热点。目前细化焊缝组织的主要方法是在焊接过程中实施的, 如变质处理^[1]、电磁搅拌^[2]等。

纳米晶体材料由于具有独特的结构特征及一系列优异的力学和物理化学性能, 因此成为材料学者研究的热点。但纳米材料制备方法本身所固有的局限性限制了其在工程上的应用, 同时也制约着对纳米材料的深入研究。实际上, 在大多数情况下, 材料在使用过程中所发生的破坏是从材料的表层开始或受材料表面性能控制, 如果能在材料上制备出纳米晶结构表层, 即实现表面纳米化, 就可以利用纳米材料的优异性能提高材料的整体性能。与其它纳米材料制备方法不同的是, 表面纳米化只需通过一些常规的表面加工技术即可实现。这些方法所获得的纳米晶表层具有高致密、少污染及与基体结合紧密的优点。目前已经研发出表面机械研磨^[3]、超声冲击^[4]等多种表面纳米化技术, 其中表面机械研磨 (SMAT) 技术获得了较多的关注。利用 SMAT 已经成

功实现表面纳米化的材料主要包括: 纯铁、钢、镁合金、铝合金、铜、钛合金等。

超声冲击作为一种消除焊接残余应力, 提高焊接结构疲劳强度的有效工艺, 近年来得到了越来越广泛的应用^[5]。超声冲击设备具有方便、灵活, 不受零件复杂结构限制, 可以适应恶劣多变的施工现场工况等优点。因此如果能够利用超声冲击技术, 在消除焊接残余应力的同时, 细化焊接接头表面层显微结构, 即实现表面纳米化, 提高焊接结构的服役性能将是非常有意义的。

文中以工程上广泛应用的 J507 堆焊层为研究对象, 采用超声冲击工艺在堆焊层表层制备纳米晶结构。同时, 应用金相显微镜、XRD、TEM 等技术对制备的纳米结构进行了表征。

1 试验方法

试验采用 20 钢板为基体材料, 板厚 15 mm, 将板材切割成 150 mm \times 150 mm 片状样品。经除锈、除油清洗后, 进行堆焊。堆焊工艺采用焊条电弧焊, 焊接速度为 10~20 mm/min, 焊接电流为 120 A, 焊条为 J507, 直径 ϕ 4.0 mm, 施焊前在烘干炉中烘干, 工艺为 380 $^{\circ}\text{C}\times$ 1 h。

表面纳米化处理采用超声冲击 (ultrasonic impact peening, UIP) 技术实现, 试验装置如图 1 所示。超声冲击表面纳米化的基本原理: 超声冲击头沿试样表

面法线方向给试样施加一定幅度的超声频机械振动,并在一定静压力和进给速度条件下,冲击头将压力和超声冲击传递给处于旋转状态的待处理试样表面,利用超声冲击作用使材料产生弹塑性变形,从而改变金属表面形貌和显微组织,并提高其综合力学性能.

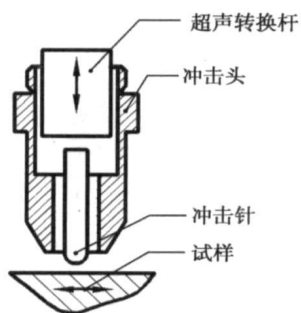


图1 超声冲击试验装置结构示意图

Fig. 1 Schematic illustration of UIP surface nanocrystallization configuration

试验采用的超声冲击频率为 20 kHz, 时间为 30 min. XRD 试验在 DMAX 2550 VB/PC 型 X 射线衍射仪上进行, 试验采用铜靶. 管压为 40 kV, 管流为 450 mA, 对有衍射峰的角度范围分段测量, 步进为 0.02° . TEM 观察在 JEOM 2010 电子显微镜上进行, 工作电压为 200 kV, 样品制备采用单面离子减薄方法. 利用金相显微镜观察超声冲击处理以后样品横截面上组织的变化, 试样采用 3% 浓度的硝酸酒精溶液腐蚀.

为了了解超声冲击表面纳米化对堆焊层性能的影响, 进行了显微硬度测试. 显微硬度测试在 HXD-1000TM 显微硬度计上进行, 载荷为 2 N, 加载时间为 30 s. 直接在样品的表面测量表面纳米层的硬度, 在样品的横截面上测量了由表面层到心部的硬度变化.

2 试验结果与讨论

J507 堆焊层经过超声冲击处理后样品横截面的金相组织如图 2 所示. 由图可见堆焊层心部是典型的焊缝组织, 为晶间铁素体和侧板条铁素体. 可以看出, 在超声冲击过程中样品表面附近发生了强烈塑性变形, 变形量随着深度的增加而逐渐减小. 最大变形深度可达 $50 \mu\text{m}$, 其中强烈塑性变形主要发生在表面到 $30 \mu\text{m}$ 深度的范围, 其组织结构在金相显微镜下已经不能分辨. 从强烈塑性变形区内金属

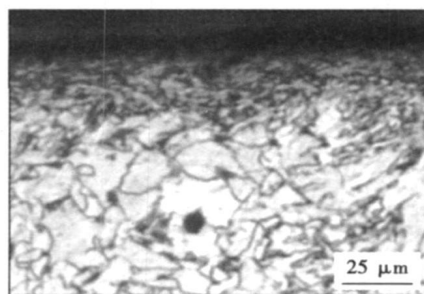


图2 J507 堆焊层经超声冲击处理后横截面组织

Fig. 2 Optical micrograph of cross-section of J507 weld processed by UIP

的流变条纹可见, 塑性变形沿各个方向随机发生, 无择优取向. 这种变形方式与 SMAT 方法制备的纳米晶表层变形方式相似, 而与等通道角挤压 (ECAP)^[9]、叠轧合 (ARB)^[7]、大应变塑性机械加工^[8] 等强烈塑性变形法制备的纳米材料中沿某特定方向发生的塑性变形有着明显的不同.

超声冲击前后 J507 堆焊层的 XRD 衍射图谱如图 3 所示. 从图中可以看出, 由于微观应变增加和晶粒细化样品的衍射峰明显宽化. 利用 XRD 数据分析所确定的晶粒尺寸和微观应变, 如表 1 所示. 样品表面的微观应变为 0.3341%, 大于 SMAT 方法获得的纳米晶材料^[9].

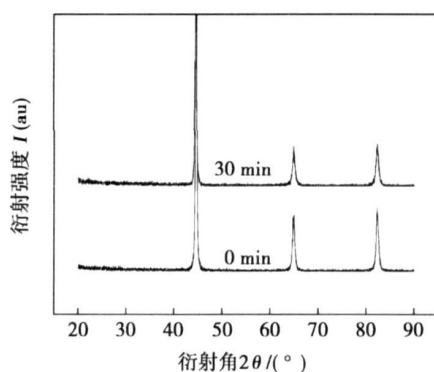


图3 J507 堆焊层超声冲击处理前后的 XRD 衍射图谱

Fig. 3 XRD diffraction pattern of J507 weld before and after UIP

表1 J507 堆焊层超声冲击处理后晶粒尺寸和微观应变

Table 1 Average grain size and mean microstrain of treated sample calculated from XRD data

衍射晶面	晶粒尺寸 s/nm	显微应变 $(\epsilon)^{1/2}(\%)$
(110)	29.36	0.3087
(200)	15.13	0.4228
(112)	19.27	0.2707
平均	21.25	0.3341

图4为超声冲击处理后样品表层的TEM明场像和选区电子衍射花样。可见样品表面晶粒已细化成纳米晶,晶粒呈等轴状。选区电子衍射表明纳米晶粒取向呈随机分布。对多张TEM像的统计表明纳米晶晶粒平均尺寸为17 nm。将TEM和XRD分析结果进行对比可以发现,TEM观测出的晶粒尺寸略小于XRD的计算结果,这主要是由于TEM薄膜试样取自样品极薄的表层($<1\ \mu\text{m}$),而XRD得到的是表面附近约 $5\ \mu\text{m}$ 厚度内的平均信息,对于表面纳米化样品来说,晶粒尺寸沿厚度方向是逐渐增大的。

在超声冲击的过程中,金属表层发生了高应变速率的严重塑性变形。 $\alpha\text{-Fe}$ 的塑性变形方式为位错运动,在外加载荷的作用下,在粗晶粒内部形成高密度的位错墙和位错缠结,通过不断地吸收位错,位错墙和位错缠结逐渐演变成小角度亚晶界,小角度亚晶界继续吸收位错而转变成大角度晶界,亚晶内部不断重复上述过程,使晶粒尺寸不断减小,取向差不断增大,最终形成等轴状、取向随机分布的纳米晶层。由于塑性应变随着距表面距离的增加而减小,导致晶粒尺寸沿厚度方向逐渐增大。

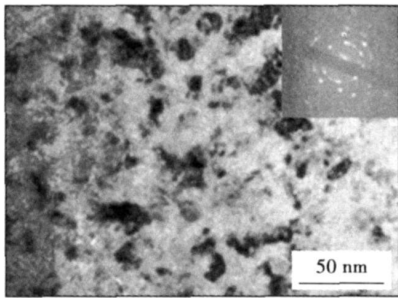


图4 J507堆焊层超声冲击处理后表面层明场TEM像和相应的选区电子衍射花样

Fig. 4 A bright-field TEM image and a corresponding SAED pattern of treated surface layer in J507 weld

图5显示出超声冲击处理后硬度沿样品厚度方向的变化。可以看出,超声冲击处理后样品表面硬度明显增大,并随着深度的增加而逐渐减小,与显微组织未发生变化的心部相比,样品表面硬度提高了1.4倍。表面以下约 $100\ \mu\text{m}$ 深度范围内的硬度也明显的增大。随着深度的进一步增加,硬度值趋于稳定。与SMAT表面纳米化相比,超声冲击表面纳米化处理后样品显微硬度的变化趋势相同,但表面纳米晶层硬度增大的幅度要小于SMAT表面纳米化处理(两倍以上)^[19]。J507堆焊层超声冲击表面纳米化强化层的厚度也要小于SMAT表面纳米化强化层厚度。产生这种现象的原因可能是由于两种工艺冲击

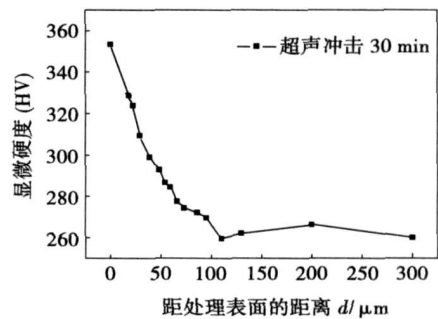


图5 超声冲击处理后显微硬度沿厚度方向的变化

Fig 5 Variation of microhardness with depth from treated surface in J507 weld treated by UIP

强度和材料本身强度不同形成的。

硬度是广泛应用的力学性能,表征金属的塑性变形抗力及应变硬化能力。在传统金属材料中硬度与晶粒尺寸的变化规律符合Hall-Petch经验公式

$$H_v = H_0 + Kd^{-1/2} \quad (1)$$

式中: H_v 为硬度; d 为晶粒直径, H_0 , K 为常数,对于普通多晶体材料 K 为正值。由Hall-Petch经验公式可知随着晶粒尺寸的减小材料变硬。

虽然在理论和试验方面都证明这种硬度与晶粒尺寸之间的依赖关系对许多金属材料在微米尺度范围是正确的,但它对于一些纳米材料并不一定成立。最近人们研究了各种方法制备的纳米材料硬度与晶粒尺寸的关系,其中包括:UFP压制、电子沉积、机械研磨、球磨、溅射、非晶晶化。随着晶粒尺寸细化到纳米量级,软化及硬化现象在试验中都观察到了。

超声冲击表面纳米化处理后J507堆焊层表面的强化可归因于晶粒细化效应和加工硬化效应共同作用的结果。尽管将两种效应进行分离还存在一定的困难,然而由样品组织与性能的对对应关系可看出,晶粒尺寸沿样品的厚度方向逐渐增大,而硬度逐渐减小。这种现象与传统的Hall-Petch关系一致,因此可认为表面组织细化对材料表层强化起主要作用。

3 结 论

(1) 采用超声冲击技术可使J507堆焊层实现表面纳米化,表面纳米晶粒尺寸为 $21.25\ \text{nm}$,表面纳米化的程度与塑性变形量有关。

(2) 表面纳米化使样品的表层明显强化,与样品的心部相比,表层的硬度可提高1.4倍,且沿样品厚度方向显微硬度逐渐减小。显微硬度的变化符合Hall-Petch关系。

参考文献:

- [1] 国旭明, 钱百年, 张 艳, 等. 外场处理细化管线钢埋弧焊缝的显微组织[J]. 焊接学报, 2001, 22(2): 27-30.
Guo Xuming, Qian Bainian, Zhang Yan, *et al.* Refining microstructure of submerged arc weld metal by using outer field treatment[J]. Transactions of the China Welding Institution, 2001, 22(2): 27-30.
- [2] 周振丰. 焊接冶金学[M]. 北京: 机械工业出版社, 1995.
- [3] Tao N R, Wang Z B, Tong W P, *et al.* An investigation of surface nanocrystallization mechanism in Fe induced by surface mechanical attrition treatment[J]. Acta Materialia, 2002, 50(18): 4603-4616.
- [4] Mordiyuk B N, Prokopenko G I. Fatigue life improvement of α -titanium by novel ultrasonically assisted technique[J]. Materials Science and Engineering A, 2006, A437(2): 396-405.
- [5] 王东坡, 霍立兴, 张玉凤, 等. 提高焊接接头疲劳强度的超声冲击法. 焊接学报[J]. 1999, 20(3): 158-163.
Wang Dongpo, Huo Lixing, Zhang Yufeng, *et al.* Enhanced fatigue strength of welded joints by means of ultrasonic impact technique[J]. Transactions of the China Welding Institution, 1999, 20(3): 158-

- 163.
- [6] Minou Furukawa, Zenji Horita, Minou Nemoto, *et al.* The use of severe plastic deformation for microstructural control[J]. Materials Science and Engineering A, 2002, 324(1-2): 82-89.
- [7] Ohsaki S, Kato S, Tsuji N, *et al.* An investigation of surface nanocrystallization mechanism in Fe induced by surface mechanical attrition treatment[J]. Acta Materialia, 2007, 55(8): 2885-2895.
- [8] Shankar M Ravi, Rao Balkrishna C, Lee Seongyeol, *et al.* Severe plastic deformation (SPD) of titanium at near-ambient temperature[J]. Acta Materialia, 2006, 54(14): 3691-3700.
- [9] Liu G, Wang S C, Lou X F, *et al.* Low carbon steel with nanostructured surface layer induced by high-energy shot peening[J]. Scripta Materialia, 2001, 44(8-9): 1791-1795.
- [10] 李 东, 陈怀宁, 刘 刚, 等. SS400 钢焊接接头表层组织纳米均一化及硬度均一化处理[J]. 金属学报, 2001, 37(9): 981-984.
Li Dong, Chen Huaining, Liu Gang, *et al.* Homogenization of microstructure and hardness of surface layer of SS400 steel welded joints[J]. Acta Metallurgica Sinica, 2001, 37(9): 981-984.

作者简介: 李 东, 男, 1974 年出生, 博士. 主要从事纳米材料及材料表面改性方面的研究. 发表论文 10 余篇.

Email: dli@ccust.edu.cn; freedomsli@yahoo.com

[上接第 95 页]

3 结 论

(1) 利用前驱体碳化复合粉末制备技术, 以蔗糖为碳的前驱体, 制备了反应等离子熔敷 Fe-Cr-C-W-Ni 复合粉末.

(2) 采用同步送粉反应等离子熔敷设备和优化的反应等离子熔敷工艺, 在调质 C 级钢基材表面制备了以原位生成初生相 $(Cr, Fe)_7C_3$ 为增强相, 以 γ 固溶体与少量 $(Cr, Fe)_7C_3$ 构成的共晶为基体的高铬铁基金属陶瓷复合涂层. 涂层组织均匀细小, 无显微孔洞和裂纹, 与基材完全冶金结合.

(3) 涂层在 900 °C 高温氧化试验条件下具有良好的抗氧化性能.

参考文献:

- [1] 刘均波, 黄继华, 王立梅. 反应等离子熔敷 Cr_7C_3/γ -Fe 金属陶瓷复合材料涂层组织与耐磨性[J]. 焊接, 2005(4): 49-52.
Liu Junbo, Huang Jihua, Wang Limei. Microstructure and wear resistance of the reactive plasma clad Cr_7C_3/γ -Fe ceramal composite coating[J]. Welding and Joining, 2005(4): 49-52.
- [2] 殷 声. 燃烧合成[M]. 北京: 冶金工业出版社, 1999.

- [3] 刘均波, 王立梅, 黄继华, 等. 离子熔覆 Cr_7C_3/γ -Fe 金属陶瓷复合材料涂层的耐磨性[J]. 机械工程材料, 2006, 30(2): 42-45.
Liu Junbo, Wang Limei, Huang Jihua, *et al.* Wear properties of plasma clad Cr_7C_3/γ -Fe ceramal composite coating[J]. Materials for Mechanical Engineering, 2006, 30(2): 42-45.
- [4] 孙荣禄, 杨贤金. 激光熔敷原位合成 TiC-TiB₂/Ni 基金属陶瓷涂层的组织和摩擦磨损性能[J]. 硅酸盐学报, 2003, 31(12): 1221-1224.
Sun Ronglu, Yang Xianjin. Microstructure friction and wear properties of in situ synthesized TiC-TiB₂/Ni based metallic ceramic coating by laser cladding[J]. Journal of the Chinese Ceramic Society, 2003, 31(12): 1221-1224.
- [5] Liu J B, Huang J H, Wang L M. Study on PTA clad $(Cr, Fe)_7C_3/\gamma$ -Fe ceramal composite coating [J]. Acta Metallurgica Sinica (English letters), 2005, 18(6): 695-700.
- [6] Liu C T, Steigler J O, Sam F H. Metals handbook[M]. 10th Edition. USA: The Materials Information Society, USA; 1990.
- [7] 刘均波. 等离子表面冶金 $(Cr, Fe)_7C_3/\gamma$ -Fe 金属陶瓷复合涂层工艺[J]. 焊接学报, 2007, 28(4): 17-20.
Liu Junbo. Process of $(Cr, Fe)_7C_3/\gamma$ -Fe ceramal composite coating formed by plasma surface metallurgy[J]. Transactions of the China Welding Institution, 2007, 28(4): 17-20.

作者简介: 王立梅, 女, 1975 年出生, 在职研究生, 实验师. 主要从事材料表面涂层技术和粉末冶金方面的研究和实验室管理工作. 发表论文 15 余篇.

Email: meiliwang620@163.com

study compositions and microstructures of the coating. The oxidation resistance of the ceramal composite coating was investigated under the testing condition of 900 °C and 50 hours. The results indicate that the excellent oxidation resistance of the coating is mainly attributed to the relatively continuous oxide scales which mainly consist of Cr_2O_3 and Fe_2O_3 , and the oxide scales can prevent the inner part of the composite coating from being further oxidized.

Key words: reactive plasma cladding; high-chromium iron-based composite coating; precursor; microstructure; oxidation resistance

Resistance spot welding microstructure proportion simulation and experiment analysis on two aluminium alloys

TANG Xinxin, SHAN Ping, LUO Zhen, LUO Baofa (College of Material Science and Engineering, Tianjin Key Laboratory of Advanced Joining Technology, Tianjin University, Tianjin 300072, China). p96–100

Abstract AA5754 and AA6082 aluminium alloy are two kinds of aluminium alloys with different strengthen modes. In the processing of the resistance spot welding, the microstructure of the two aluminium alloys changes in different types. By two different numerical models, the microstructure proportion in the nuggets of the two aluminium alloys was simulated and predicted. Compared with the experimental results, the two simulation models are effective to predict some important phenomenas in terms of the phase transformation of the nuggets. Both the simulation results and the experimental results show that there are marked different features in the phase transformation of the two kinds of aluminium alloys.

Key words: aluminium alloy; resistant spot welding; numerical simulation; welding microstructure

Fabrication and characterization of nanostructured surface layer of J507 weld by ultrasonic impact peening

LI Dong, FAN Zhao, LIAO Libao, ZHANG Li, XU Hong (State Key Laboratory of Chemical Engineering, School of Mechanical and Power Engineering, East China University of Science and Technology, Shanghai 200237, China). p100–104

Abstract: A nanostructured surface layer was fabricated on a J507 weld metal by ultrasonic impact peening (UIP). The refined microstructure in the top surface layer was characterized by means of X-ray diffraction and transmission electron microscopy (TEM), and the microhardness variation along the depth of the treated sample was examined. Experimental results show that after the UIP treatment, the microstructure of the surface layer may be refined into 21–25 nm. Grains refinement involves formation of dense dislocation walls (DDWs) and dislocation tangles (DTs) in coarse grains, transformation of DDWs and DTs into subboundaries, and evolution of subboundaries to highly misoriented grain boundaries. The strengthened thickness of the layer is 100 μm after UIP treatment. The microhardness of nanocrystalline surface layer is enhanced significantly after

the UIP treatment compared with that of the original sample.

Key words: J507 weld; ultrasonic impact peening; surface nanocrystallization; microhardness

Analysis on the tendency of welding hot cracks of aluminum alloy increased by longitudinal pre-tension

ZHOU Guangtao¹, LIU Xuesong¹, YANG Jianguo¹, FANG Hongyuan^{1,2} (1. State Key Laboratory of Advanced Welding Production Technology, Harbin Institute of Technology, Harbin 150001, China; 2. Institute of Astronautical Technology, Shenyang Institute of Aeronautical Engineers, Shenyang 110034, China). p105–108

Abstract Numerical simulation calculation of TIG welding of thin wall aluminum cylinder by the thermo-elastic FEM has been conducted. Based on the generating of analysis model, the values and distribution at the centre of weld seam for transverse tensile stress and strain produced by pre-tension upon the solidification metal at the back of molten pool. Experiments were performed to verify the simulation results. It can be drawn that for weld metal just solidified at the joint pre-tension load can produce transverse tensile stress, which increases the tendency of welding hot cracks. And with the increasing of pre-tension load, the transverse tensile stress increases. When the pre-tension stress is 60, 120, 150 and 210 MPa, the crack length in specimens is 5.2 mm, 8.1 mm, 8.9 mm and 10.6 mm, respectively. The tests results indicates the reliability of simulation results.

Key words: pre-tension; numerical simulation; residual stress; hot cracks

Effects of M-A constituent on toughness of coarse grain heat-affected zone in HSLA steels for oil tanks

ZHANG Yingqiao¹, ZHANG Hanqian^{1,2}, LIU Weiming¹ (1. Department of Materials Science and Engineering, Shanghai Jiaotong University, Shanghai 200030, China; 2. Research Institute for Advanced Structural Steel, R&D Center, Baoshan Iron and Steel Limited Company, Shanghai 201900, China). p109–112

Abstract Microstructure and impact toughness of CGHAZ in HSLA steels for oil tanks under high heat input (100 kJ/cm) have been investigated. Bainite is main microstructure in CGHAZ for four steels but there is a significant difference in impact values due to different proportion of ferrite and granular bainite. Toughness values decrease with the increase of area percentage content of M-A constituents. The effects of morphology of M-A constituents on toughness have also been studied and the harm of massive M-A constituent is more severe than that of long strip. Considering the influence of alloy elements on the formation of M-A constituents, area percentage contents of M-A constituents are predicted by the method of multiple linear regressions, which is helpful for evaluating the toughness of CGHAZ.

Key words: heat input; coarse grain heat-affected zone; M-A constituent; impact toughness